EPR and ENDOR Studies of 1 H and 14 N Hyperfine and Quadrupolar Couplings in Crystals of l - O Serine Phosphate after X-Irradiation at 295 K

ARTICLE *in* THE JOURNAL OF PHYSICAL CHEMISTRY · MAY 1996

Impact Factor: 2.78 · DOI: 10.1021/jp960063x

2 AUTHORS:

Audun Sanderud
Norwegian Radiation Protection Authority
29 PUBLICATIONS **169** CITATIONS

SEE PROFILE

Einar Sagstuen
University of Oslo
176 PUBLICATIONS **2,393** CITATIONS

SEE PROFILE

EPR and ENDOR Studies of ^{1}H and ^{14}N Hyperfine and Quadrupolar Couplings in Crystals of L-*O*-Serine Phosphate after X-Irradiation at 295 K

Audun Sanderud* and Einar Sagstuen

Department of Physics, University of Oslo, P.O. Box 1048 Blindern, N-0316 Oslo, Norway

Received: January 2, 1996; In Final Form: March 7, 1996[⊗]

Single crystals of L-*O*-serine phosphate, $(HOOC)CH(NH_3^+)CH_2OPO_3^-H$, were X-irradiated at 295 K and studied using EPR, ENDOR, and FSE techniques. At this temperature, three carbon-centered radicals were identified. Radical **I**, the deamination product $(HOOC)\dot{C}HCH_2OPO_3^-H$, is shown to have undergone a major molecular reorientation upon formation. Radical **II** is identified to be the product $(HOOC)CH(NH_3^+)\dot{C}HOPO_3^-H$. This species exhibits a nonplanar site for the lone electron density. This deviation from planarity is ascribed to electrostatic interaction between the lone electron orbital and lone pairs centered on the neighboring oxygen atom. Hyperfine interaction with the β-nitrogen of the amino group is observed. Both the ^{14}N hyperfine and quadrupole coupling tensors are determined and the signs of the hyperfine coupling tensor principal values are deduced from interpretation of the quadrupole tensor employing the Townes−Dailey approach. The $\beta^{14}N$ isotropic interaction is well described by a Heller and McConnell type $\cos^2\theta$ rule. The results found in the present work, together with other recent observations, yield estimated values of the constants $B_0 = 1.0$ MHz and $B_2 = 34.5$ MHz. Radical **III** exhibits the structure $(HOOC)CH(NH_3^+)\dot{C}H_2$, formed by scission of the phosphate−ester bond at the carbon side. No $\beta^{14}N$ coupling is observed for this radical due to a dihedral angle close to 90°. Possible mechanistic routes for the formation of these radicals are discussed in comparison with previously published data on serine and other alkyl phosphate derivatives.

1. Introduction

The mechanisms leading to radiation-induced breaks of the phosphodiester bond in DNA has been subject to numerous investigations, in part by EPR and ENDOR spectroscopy.[1] Radiation damage by direct effects to DNA has been shown mainly to produce primary ionization of the aromatic bases, but phosphate radicals have not been observed in irradiated DNA.[2,3] There is, however, experimental evidence that the primary ionic sites on DNA are precursors to strand breaks.[2,4] The mechanisms by which base damage is transferred to the sugar−phosphate region of DNA resulting in breakage of the sugar−phosphate bonds are still largely unknown. It is believed that radical transfer to the C_4' position of the deoxyribose moiety is involved, but few details about this process are known.[1]

Several model systems have been investigated to elucidate the influence of various substituents to alkyl phosphate derivatives on the release of inorganic phosphate or phosphate-centered radicals.[5−8] Bungum *et al.*[5] studied X-irradiated disodium and dipotassium salts of glucose-1-phosphate, finding evidence for secondary loss of phosphoryl radicals, probably *via* a carbon-centered radical precursor. The same products were found[6] in the barium salt of glucose-6-phosphate and the disodium salt of β-glycerol phosphate. However, in X-irradiated disodium and barium salts of ribose-5-phosphate, the disodium salt of α-glycerol phosphate, and the monosodium salt of glucose-6-phosphate, phosphoryl radicals were not detected.

In X-irradiated *O*-phosphorylethanolamine (PEA), $(NH_3^+)CH_2CH_2OPO_3^-H$, Fouse *et al.*[7] have reported the presence of secondary phosphoryl radicals, resulting from cleavage of the $(NH_3^+)CH_2CH_2O-PO_3^-H$ phosphate ester bond. Dissociative electron capture at the bond is the assumed mechanism. In the same system Fouse *et al.*[7] reports possible cleavage of the $(NH_3^+)CH_2CH_2-OPO_3^-H$ bond, resulting in a carbon-centered radical. The concentration of the two radicals is equal.

Sørnes *et al.*[8] have investigated room-temperature radical formation by X-irradiation of aminoethyl hydrogen sulfate (AES), where the phosphate group of PEA has been replaced by the slightly more electronegative sulfate group. The studies reveal the presence of a sulfite radical, while cleavage of the $(NH_3^+)CH_2CH_2-OSO_3^-$ oxygen−ethyl bond is not observed. This difference between AES and PEA is mainly ascribed to the increased electron affinity of sulfur as compared to phosphorus.

L-*O*-serine phosphate (SP), $(HOOC)CH(NH_3^+)CH_2OPO_3^-H$, consists of the PEA system with a carboxyl group added. From previous studies of amino acids, the carboxyl group is known to be an electron sink just as efficient as the aromatic bases in DNA. Our recent experiments have shown that, as in DNA, no phosphate-centered radicals are observed in SP.[6] It was of interest to see if net dephosphorylation still occurs, and in fact, the present work shows the cleavage of the $(HOOC)CH(NH_3^+)CH_2-OPO_3^-H$ phosphate ester bond takes place. Thus, it seem that the presence of an electron scavenger in the system prevents the formation of phosphate-centered radicals, but not cleavage of the phosphate ester bond at the carbon side.

In the present paper three carbon-centered radicals formed by X-irradiation in SP at room temperature are identified. The corresponding radicals are observed in serine,[9,10] and it is suggested that similar radical reactions lead to the observed room-temperature radicals in the two compounds.

2. Experimental Section

Single crystals of L-*O*-serine phosphate (SP) were grown from warm (40 °C) saturated aqueous solutions by slow cooling. Partially deuterated samples were similarly prepared by repeated recrystallization from 99.8 g/100 g purity deuterium oxide solutions. The crystal structure of SP has been analyzed by Sundaralingam and Putkey.[11] The unit cell is orthorhombic with space group $P2_12_12_1$ and $Z = 4$.

* Author to whom all correspondence should be addressed.

[⊗] Abstract published in *Advance ACS Abstracts,* May 1, 1996.

S0022-3654(96)00063-9 CCC: $12.00

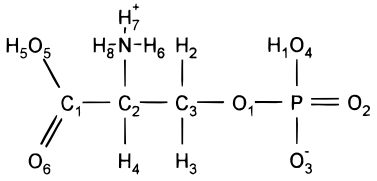

L-*O*-serine phosphate

The crystals were irradiated at 280 K using X-rays from a tungsten target tube operated at 60 kV and 50 mA, such that each sample received a total dose of 50 kGy at about 30 kGy/h. The crystals were aligned along each crystallographic axis using a Weissenberg X-ray diffraction camera and subsequently transferred to a quartz sample holder without loss of axis alignment. First-derivative room-temperature data were collected at X-band microwave frequencies with a Bruker ER-200 D-SRC spectrometer with and EN-200 ENDOR unit equipped with a 100 W ENI rf-amplifier, in 5° intervals through more than 90° in each plane. At each orientation the ENDOR frequency was swept from 1 to 75 MHz in 10 or 50 MHz intervals.

The proton hyperfine coupling (hfc) tensors were determined using the program MAGRES,[12] while the ^{14}N hyperfine and quadrupolar coupling (nqc) tensors were found using the program NQENDFIT.[8] In both cases isotropic *g*-tensors were assumed (see below).

3. Results

3.1. EPR Spectroscopy. Figure 1 shows the EPR spectra obtained with the magnetic field directed along each of the crystallographic axes. The spectra in Figure 1a are from crystals grown in aqueous solution, while spectra in Figure 1b are from partially deuterated samples. There are only small differences between the spectra from the two kinds of crystals, indicating that the major hyperfine couplings are due to interaction with carbon-bonded protons or the nitrogen atom. When the crystals were stored at room temperature for 3−4 months, the resonance shown in Figure 1a disappeared and the spectra shown in Figure 1c were observed. The ENDOR experiments show that the resonance is present initially, but hidden under the far more intense resonance depicted in Figure 1a.

Since the EPR spectra contain contributions from several radicals, they were difficult to analyze. The ENDOR analyses, however, gave good results, and radical structures were determined without further use of the EPR results other than establishing that the resonances exhibit virtually isotropic *g*-tensors.

3.2. ENDOR Spectroscopy. The ENDOR spectra revealed eight hyperfine couplings which could be followed through all three rotation planes. The angular variations of these couplings are shown in Figures 4, 5, and 8. From these data seven proton hfc tensors and one ^{14}N hfc tensor with an nqc tensor were determined. FSE (field-swept ENDOR) experiments showed that these couplings could be ascribed to three different radicals: one major radical (radical **I**) and two less abundant species (radicals **II** and **III**).

Figure 2 shows the ENDOR spectra obtained with the magnetic field along the crystallographic *b*-axis both for protiated (Figure 2a) and for partially deuterated crystals (Figure 2b). The spectrum in Figure 2a contains resonance lines from couplings for which the hfc tensors could not be determined because of difficulties following the resonance lines through all three rotation planes. In the spectrum from the deuterated crystal (Figure 2b) some of the lines present in Figure 2a are missing. These resonance lines are thus due to couplings with

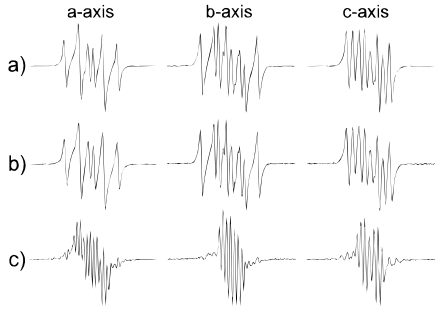

Figure 1. First derivative EPR spectra (width 20.0 mT, centered at $g_e = 2.0023$) of L-*O*-serine phosphate single crystals, X-irradiated at 280 K and then measured at room temperature. The spectra in part a are recorded using crystals grown in water, in part b the spectra are recorded using partially deuterated crystals, and in part c they are recorded using crystals grown in water stored for 4 months after X-irradiation. The spectra are measured with the external magnetic field along the indicated crystal axes.

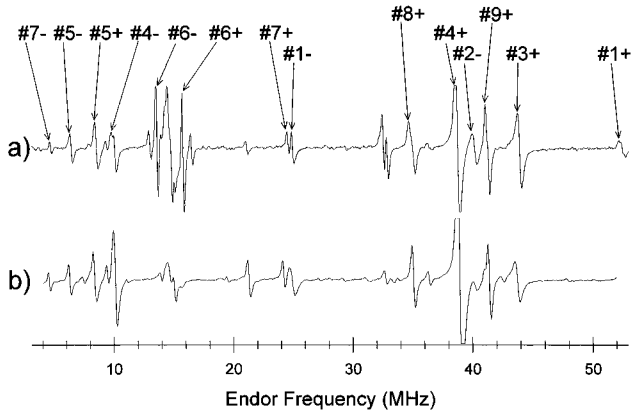

Figure 2. First derivative ENDOR spectra of L-*O*-serine phosphate single crystals freshly X-irradiated at 280 K and measured at room temperature. The spectra are recorded with the external magnetic field oriented along the crystallographic *b*-axis. Spectrum a is from a crystal grown in water, while b is obtained from a partially deuterated crystal. The high-branch (+) and low-branch (−) ENDOR transitions from which hfc or nqc tensors were calculated are indicated by numericals. Line #1+ is not visible in part b because the spectrum has a slightly shorter range than the spectrum in part a.

easily exchangeable protons. For one of these exchangeable couplings (designated #6) the hfc tensor was determined (Table 2).

Hyperfine coupling tensors based on data from rotations around three orthogonal axis leave an ambiguity in the signs of the off-diagonal tensor elements. Schonland[13] pointed out that this could be resolved by investigating a plane of data using a skewed axis of rotation. This has been done for most of the tensors obtained in this work. Figure 3 shows typical results from a skewed axis rotation plane ($\theta = 45°$, $\phi = 90°$) displaying results for hfc tensor #4. Here, the fully drawn and stipled curves are calculated from the two different hfc tensors given by the Schonland ambiguity. It is clear that only one of the two tensor alternatives reproduces the experimental result. This method was used for tensors #1, #3, #4, #8, and #9 in this work. For the other tensors, the differences between the two tensor alternatives were too small and indirect arguments were used to settle on those chosen in Table 1 (see below).

3.3. Radical I. FSE was used to assign the ENDOR lines in Figure 2 to three different radicals. Radical **I** is the major species. As described above, the EPR due to this radical slowly disappeared upon storage at room temperature. Three proton ENDOR resonance lines (#1, #2, and #3) were assigned to this radical, as demonstrated in Figure 4. These ENDOR lines were

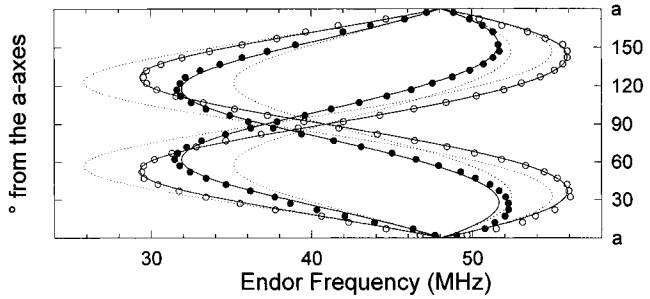

Figure 3. Calculated and observed ENDOR frequency variation through the skew axis rotation plane for hfc tensor #4 from L-*O*-serine phosphate single crystals freshly X-irradiated at 280 K. This plot allows the determination of the signs of the off-diagonal elements of the hfc tensor. The axis of rotation is given by the polar angles $\theta = 45°$ and $\varphi = 90°$. The fully drawn and the dotted lines represent the calculated variations for the two different sets of sign alternatives obtained from the tensor given in Table 2. The filled and open circles represent experimental data for the two different molecular sites.

TABLE 1: Hyperfine Coupling Tensors for Radical I in Single Crystals of L-*O*-Serine Phosphate X-Irradiated at 280 K[a]

tensor	principal values (MHz)	isotropic value (MHz)	direction cosines ⟨*a*⟩	⟨*b*⟩	⟨*c*⟩
αH	−86.5	−54.2	0.559	−0.819	−0.130
(#1)	−50.9		0.829	0.549	0.102
	−25.2		0.012	0.164	−0.986
*β*H	111.5	104.3	0.063	−0.936	0.349
(#2)	102.3		0.786	0.261	0.561
	99.0		0.616	−0.237	−0.752
*β*H	65.5	57.4	0.773	−0.617	−0.150
(#3)	53.5		0.633	0.767	0.107
	53.2		0.049	−0.177	0.983

[a] The errors involved in the principal values and eigenvectors are about ±0.2 MHz and ±3°, respectively.

all characterized by fading upon storage at room temperature. The hfc tensors for these three couplings are given in Table 1.

The three proton hfc tensors were used to simulate the EPR absorption spectra measured along the crystallographic *a*- and *b*-axes. These simulated spectra were compared with the experimental FSE spectra at these orientations, and the three proton couplings fully reproduce the splitting pattern in the FSE spectra.

3.4. Radical II. After the disappearance of radical **I**, the dominant radical responsible for the spectra in Figure 1c is radical **II**. The FSE spectra were used to assign two proton hfc's (#4, #6) and the ^{14}N coupling (#5) to this radical, as shown in Figure 5. Coupling #6 is to a proton which is exchanged with deuterium in the deuterated crystals. The proton and nitrogen hfc tensors are given in Table 2.

The FSE spectrum from the high-frequency ENDOR line of coupling #4 at the *c*-axis orientation clearly shows seven lines. A stick diagram was constructed from the hfc tensors of radical **II**, Table 2. To account for this FSE spectrum, it was necessary to include one extra proton coupling. This additional coupling was calculated from the FSE spectra to be 0.62 mT at this orientation of the crystal. In the same way it was necessary to include an extra coupling to explain the FSE along the other two axes, *a* and *b*. At these orientations, the extra coupling was calculated to be 1.39 and 0.63 mT, respectively. For the *b*-axis orientation this corresponds to ENDOR lines at 5.8 and 23 MHz. In Figure 2 there clearly are ENDOR lines present which fit these expectations. It was not possible to obtain a full hfc tensor for this coupling, but from a few observations

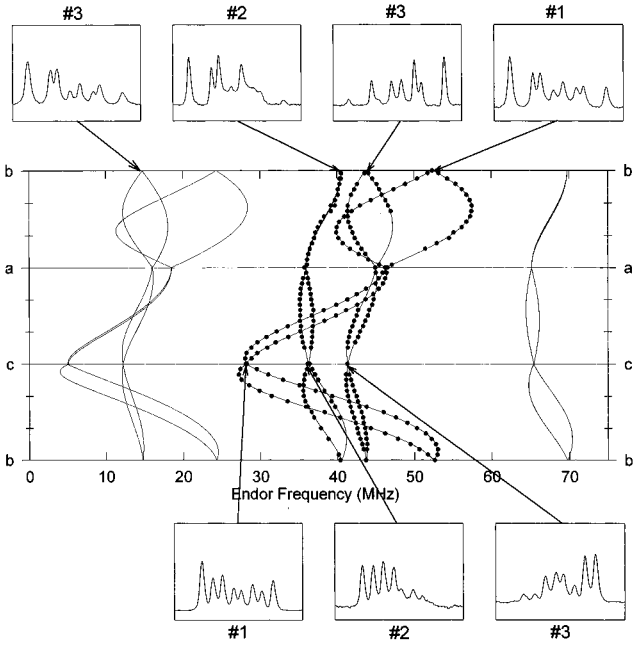

Figure 4. Angular variations of the high-branch (+) ENDOR transitions from the proton couplings #1, #2, and #3 of radical **I** in L-*O*-serine phosphate single crystals freshly X-irradiated at 280 K. The FSE spectra (width 11.8 mT, centered about $g_e = 2.0023$) connecting these couplings to one radical are shown. The solid curves represent the angular variations calculated from the coupling tensors listed in Table 1.

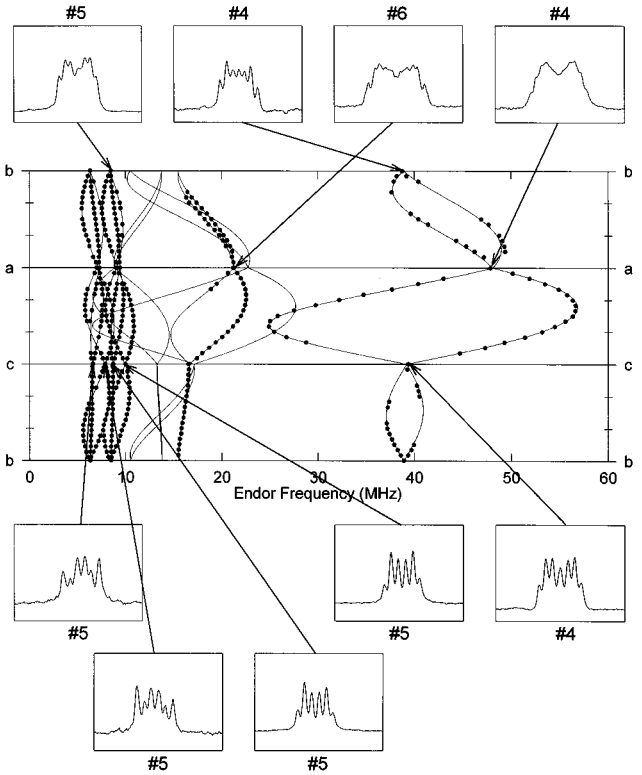

Figure 5. Angular variations of the ENDOR transitions from proton couplings #4 and #6 and the ^{14}N coupling #5 of radical **II** in L-*O*-serine phosphate single crystals X-irradiated at 280 K. The FSE spectra (width 11.8 mT, centered about $g_e = 2.0023$) connecting these couplings to one radical are shown. The solid curves represent the angular variations calculated from the coupling tensors listed in Table 2.

an estimate for the coupling was obtained. This estimated tensor is included in Table 2 (#7). The coupling is nonexchangeable and assumed to be of *β*-type.

TABLE 2: Hyperfine Coupling Tensors and the Quadrupolar Coupling Tensor of the ^{14}N Coupling for Radical II in Single Crystals of L-*O*-Serine Phosphate X-Irradiated at 280 K[a]

tensor	principal values (MHz)	isotropic value (MHz)	direction cosines ⟨*a*⟩	⟨*b*⟩	⟨*c*⟩
αH	−85.5	−51.0	0.799	−0.177	0.581
(#4)	−47.2		0.107	0.982	0.153
	−20.3		0.598	0.059	−0.799
βN(#5)	17.95	15.89	0.613	0.411	0.675
hfc	15.62		0.738	0.007	−0.675
	14.07		0.282	−0.911	0.299
βN(#5)	0.904		0.529	0.378	0.760
nqc	−0.281		0.078	−0.913	0.400
	−0.623		0.845	−0.152	−0.512
γH	16.0	5.9	0.773	−0.617	−0.150
(#6)	1.8		0.633	0.767	0.107
	0.1		0.049	−0.177	0.983
βH	39	25		∼*a*-axis	
(#7)	18			∼*b*-axis	
	17			∼*c*-axis	

[a] The errors involved in the principal values and eigenvectors are about ±0.2 MHz and ±3°, respectively, for the proton tensors. For the ^{14}N coupling tensors the corresponding errors are ±0.01 MHz and ±1°, respectively.

3.5. The ENDOR/FSE Test. The FSE spectra obtained by monitoring the ENDOR lines due to the ^{14}N coupling show only six lines at the *c*-axis orientation, while the FSE spectra obtained by monitoring the ENDOR lines due to the proton couplings of the same radical show seven lines. This is due to the fact that ^{14}N has nuclear spin $I = 1$. Some of the EPR transitions are therefore not present in the FSE spectra, dependent on which ENDOR transitions are monitored and upon the relative signs of the quadrupole and the hyperfine coupling of ^{14}N . For the same reason, some ENDOR transitions are not present depending on which EPR transitions of the ^{14}N manifold are monitored. This was discussed in detail in a previous paper by Sørnes *et al.*[8]

Figure 6 shows ENDOR spectra obtained by monitoring different EPR lines with different ^{14}N spin quantum numbers (positions 1 and 3 correspond to $m_I = \pm 1$, and position 2 corresponds to $m_I = 0, \pm 1$), and Figure 7 shows FSE spectra obtained by monitoring different ENDOR transitions. Both these experiments lead to the conclusion that the quadrupolar and hyperfine couplings must have different signs at this orientation. The analysis of the nqc tensor given below suggests that the nitrogen hfc is positive. Together, this yields the hfc and nqc tensors presented in Table 2.

3.6. Radical III. The two last proton hfc's for which coupling tensors were determined (#8 and #9) exhibit ENDOR lines which easily were followed through the three planes of rotation. The FSE spectra were characteristic, as shown in Figure 8, and unambiguously connect the two ENDOR lines to the resonance of one radical. The hfc tensors obtained, assigned to radical **III**, are given in Table 3.

The FSE spectra recorded along, for example, the *b*-axis exhibit five lines. To accomplish this, at least three proton hfc's are needed. Consequently, one further coupling must be associated with radical **III**, which has not been possible to obtain from the ENDOR data. The FSE spectrum along the *b*-axis was reconstructed by adding either one additional proton coupling of 2.55 mT or a ^{14}N coupling of 1.28 mT. Both these alternatives yield a satisfactory reconstruction of the FSE spectra. The proton coupling should give rise to ENDOR lines at 50.3 and 21.1 MHz, and the ^{14}N coupling should (if quadrupolar splitting is neglected) give ENDOR lines at 19.0 and 21.2 MHz. In Figure 2 there is an ENDOR line at ∼21 MHz, but it has not been possible to follow this line through the three rotation planes so that a tensor could be calculated. However, it is

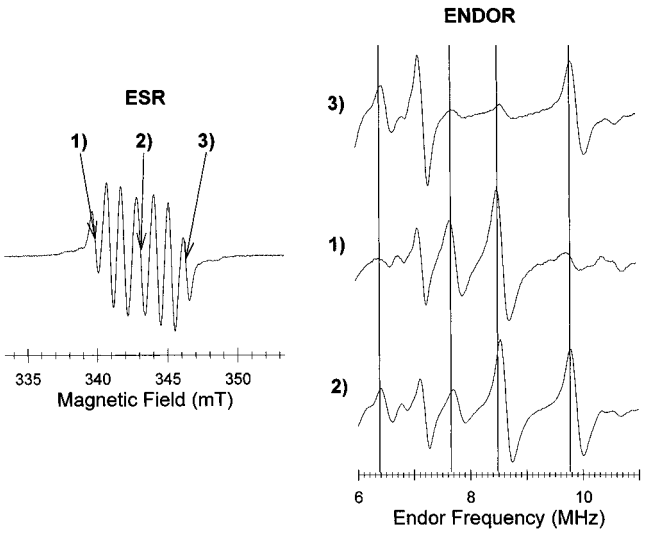

Figure 6. EPR/ENDOR test. To the left the first derivative EPR spectrum from L-*O*-serine phosphate single crystals X-irradiated at 280 K is shown. The magnetic field is directed along the crystallographic *c*-axis. The field positions 1, 2, and 3 where the magnetic field has been locked during the recording of the ENDOR spectra 1, 2, and 3 to the right are indicated. In spectrum 2, recorded off the central position of the EPR spectrum, all four ENDOR lines are present, while in spectrum 1 only the two inner ENDOR transitions and in spectrum 3 only the two outer ENDOR transitions are present. This experiment shows that the signs of the hyperfine and quadrupolar coupling are the same at this orientation of the crystal. The ENDOR line at 7.18 MHz is due to an unidentified coupling.

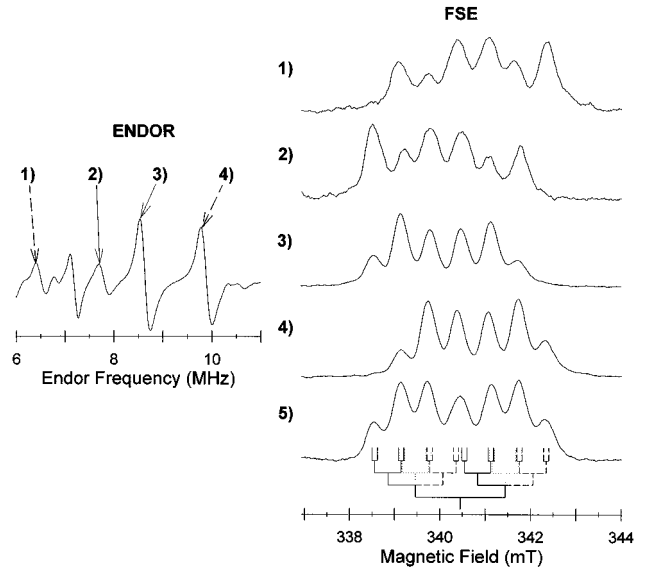

Figure 7. ENDOR/FSE test. In the ENDOR spectrum to the left the positions 1, 2, 3, and 4 indicate the monitoring frequencies used while recording the FSE spectra 1, 2, 3, and 4 to the right. For reference, spectrum 5 is the entire FSE spectrum recorded off the high-frequency ENDOR line of coupling #4. In the FSE spectra 2 and 3, recorded off the inner ^{14}N ENDOR transitions, the high-field line of the FSE spectrum is missing, while in the FSE spectra 1 and 4 the low-field line is missing. This shows, similarly to the results in Figure 6, that the signs of the hyperfine and quadrupolar coupling are the same at this orientation. The different lines in the stick diagram represent different m_I quantum numbers, and for a positive nitrogen hyperfine coupling the solid lines represent $m_I = +1$; the dotted lines, $m_I = 0$; and the stippled lines, $m_I = -1$.

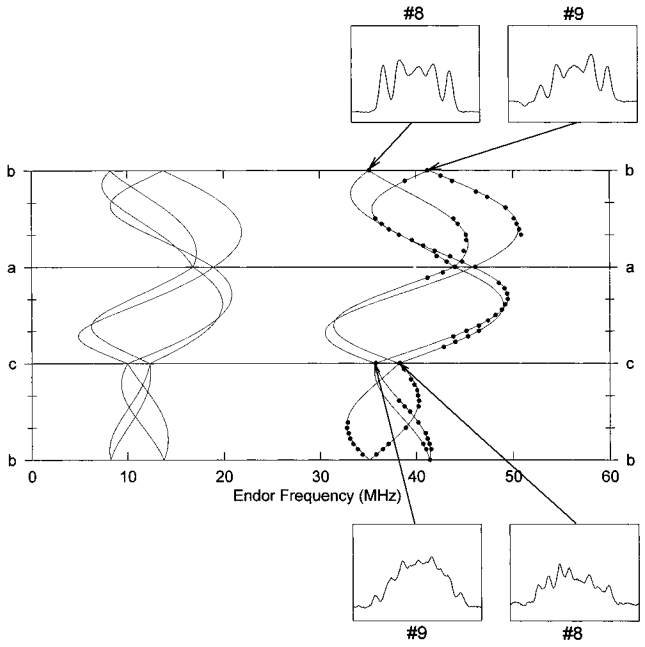

Figure 8. Angular variations of the high-branch (+) ENDOR transitions from the proton couplings #8 and #9 of radical **III** in L-*O*-serine phosphate single crystals X-irradiated at 280 K. The FSE spectra (width 11.8 mT, centered about $g_e = 2.0023$) connecting these couplings to one radical are shown. The solid curves represent the angular variations calculated from the coupling tensors listed in Table 3.

TABLE 3: Hyperfine Coupling Tensors for Radical III in Single Crystals of L-*O*-Serine Phosphate X-Irradiated at 280 K[a]

tensor	principal values (MHz)	isotropic value (MHz)	direction cosines ⟨*a*⟩	⟨*b*⟩	⟨*c*⟩
αH	−69.1	−47.1	0.829	0.114	0.548
(#8)	−48.6		0.254	0.795	−0.550
	−23.5		0.499	−0.595	−0.630
αH	−75.4	−50.8	0.812	−0.475	−0.338
(#9)	−50.3		0.214	0.782	−0.586
	−26.6		0.543	0.404	0.736

[a] The errors involved in the principal values and eigenvectors are about ±0.2 MHz and ±3°, respectively.

clear that one extra coupling in addition to the two found by ENDOR is required. This will be discussed further below (section 4.4).

4. Discussion of Radical Structure

4.1. Radical I. Three hfc tensors, designated #1, #2, and #3 in Table 1, have been shown to be associated with radical **I**. Tensor #1 exhibits principal values with typical α-character, while tensors #2 and #3 are typical β-type tensors. All couplings are clearly due to protons which are not exchanged with deuterons in the partially deuterated crystal. In SP the only nonexchangeable protons are H2, H3, and H4. Therefore, the only possible location for the main density of the lone electron orbital, LEO, is C2. Furthermore since no α-nitrogen hfc is observed, it is assumed that radical **I** is formed by a net deamination process and exhibits the structure

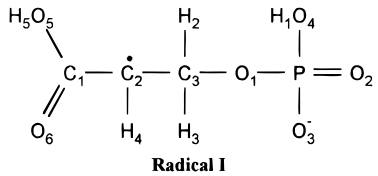

Radical I

TABLE 4: Crystallographic Directions As Determined by Sundaralingam and Putkey[10] between C2 and H2, H3, H4, and N in Single Crystals of L-*O*-Serine Phosphate[a]

direction	crystallographic	experimental #3	experimental #2	difference #3	difference #2
C2−H2	0.800	0.773	0.043	2.68°	51.2°
	−0.590	−0.617	−0.938		
	0.111	0.150	0.345		
C2−H3	0.897	0.7773	0.043	26.1°	66.9°
	0.241	0.617	0.938		
	0.370	0.150	0.345		
C2−H4	−0.442	−0.012		26.9°	
	−0.276	−0.164			
	0.853	0.986			
C2−N	0.418	0.829		44.5°	
	0.530	0.549			
	0.738	0.102			

[a] These directions are compared with corresponding experimental eigenvectors for the hfc tensors of radical **I**. In each case, the signs of the direction cosine elements of the eigenvectors are chosen so as to minimize the angular deviation.

Upon deamination of SP, the C2 atom is assumed to rehybridize to a planar sp^2 configuration, mostly by reorientation of H4. An indication of the degree of rehybridization may be obtained by comparison of two methods for finding the $2p^\pi$ spin density at C2 from the α-coupling tensor #1. One method consists of using the isotropic value, $a_{iso} = -54.2$ MHz, in the McConnell relation[14] with $Q^H_{CH} = -73.4$ MHz[15] for a planar sp^2 configuration.[16] This gave $\rho^\pi_{iso} = 0.738$. The other method consists of using the dipolar part of the α-coupling tensor #1 in the Gordy−Bernhard method,[17] giving $\rho^\pi_{dip} = 0.749$ with $Q^{dip}_z = 38.7$ MHz. The similarity of these two values confirms sp^2 configuration at C2.

The dihedral angles θ_2 and θ_3 of the two β-protons (tensors #2 and #3) with respect to the LEO are found by the Heller−McConnell relation[18]

$$a_{iso} = \rho^\pi(B_0 + B_2 \cos^2 \theta) \qquad (1)$$

For aliphatic systems the constants B_0 and B_2 in this relation are given by a B_0 between ±14 MHz and $B_2 \approx 126$ MHz.[19] The isotropic value of coupling #2 is very large, and to obtain $\theta_2 = 0°$ with a spin density as found above, B_0 must be set to 13.3 MHz. This in turn gives the dihedral angle for coupling #3, $\theta_3 = 135.2°$. The C3 atom is expected to maintain its near sp^3 hybridization configuration, and the difference between the two dihedral angles θ_2 and θ_3 should therefore be 120°. Using this as a constraint, the $2p^\pi$ spin density at C2 according to the Heller−McConnell relation should be as large as 0.782, and the corresponding dihedral angles become $\theta_2 = 13.3°$ and $\theta_3 = 133.3°$. This probably implies that B_2 is somewhat underestimated, but nevertheless gives a useful estimate of the dihedral angles.

The crystallographic unit cell space group $P2_12_12_1$ with $Z = 4$ implies that each of the four possible unique combinations of signs of each direction cosine element of an eigenvector {(*l*,*m*,*n*), (*l*,*m*,-*n*), (*l*,-*m*,*n*), and (*l*,-*m*,-*n*)} corresponds to one of the four molecular sites in the crystal. For a structural discussion, it is important to be certain that the set of eigenvectors used for all hfc tensors of a given radical are referred to the same molecular site. In the absence of more detailed experimental observations, the sets of eigenvectors to be chosen are obtained by comparison with specific crystallographic directions. The guidelines used are that the eigenvector for the α-proton minimum principal value corresponds to the C−H_α bond direction, the eigenvector

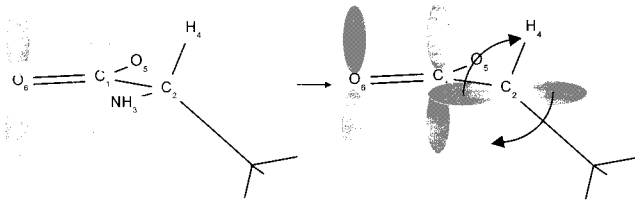

Figure 9. Structure of the O6−C1−C2−N fragment in L-*O*-serine phosphate single crystals. The left side illustrates that the O6, C1, C2, and N atoms are situated in the same plane and highlights the $2p_z$ orbitals of O6 and C1. Upon deamination forming radical **I**, the right side shows how the LEO will tend to get parallel with the two $2p_z$ orbitals so as to increase the conjugation between C2 and C1−O6.

for the intermediate principal value for the α-proton corresponds to the direction of the LEO, and the eigenvector for the maximum principal value for a β-proton nearly corresponds to the C···H_β direction. In Table 4 the crystallographic direction for the C2−H2 bond and the crystallographic C2−H3, C2−H4, and the C2−N directions are compared with experimental eigenvectors. In each case the sign of each direction cosine is chosen so as to minimize the calculated angle of deviation. The crystallographic directions (except C2−H4) are expected to be conserved in the radical if reorientation of radical **I** is restricted to rehybridization at C2.

Except for the case of tensor #3 and the C2−H2 direction, all other crystallographic directions fit poorly with the experimental eigenvectors. A more extensive molecular reorientation must therefore be assumed to occur upon radical formation to explain the hfc tensors. A larger reorientation has also been observed for the corresponding radical in single crystals of serine.[10]

This reorientation can be explained from the hydrogen-bonding pattern in the SP crystal. The crystal structure shows five unique hydrogen bonds[11] (hb's), so that every SP molecule is involved with 10 hb's. Three of these are associated with the amino group, five with the phosphate group, and two with the carboxyl group. The amino group is therefore important as an anchor, holding the molecule fixed in the crystalline lattice. When this group is lost, as in radical **I**, a displacement of the C2 atom becomes possible.

A close examination of the structure of SP reveals that a reorientation is not only possible but also highly likely. The atoms of the fragment N−C2−C1−O6 are situated almost in the same plane (the torsion angle between planes N−C2−C1 and C2−C1−O is only 2.6°), and one of the bonds between O6 and C1 is a $2p_\pi$ bond, as shown in Figure 9a). When the amino group is lost, the resulting LEO at C2 will tend to become parallel with the two $2p_\pi$ orbitals and increase the conjugation with C1−O6, as illustrated in Figure 9b.

If this reorientation occurs with the remaining hb's intact, it must take place by torsion about the P−O1 and the O1−C3 bonds and rotation about the O5−C1 bond. The sp^3 configuration of C3 will by this be preserved and thereby also the angles between C2 and the protons H2 and H3. This constraint is thus used to determine the choice of signs of eigenvector components for the three hfc tensors involved (Table 1). In Table 5 the resulting angles are shown, together with those calculated from crystallographic data. The experimental angles are calculated on the basis that C2 exhibits a perfect sp^2 configuration with ∠C3−C2−H4 = 120°. It should be noted that these results predict a fairly large reorientation of a part of the SP molecule upon radical formation. The new and the old C2−C3 bond directions differ by 52.8°, whereas the new and the old C2−C1 bond directions differ by 36.1°.

TABLE 5: Mutual Angles between the Directions from C2 to H2, H3, and C3 for Single Crystals of L-*O*-Serine Phosphate, As Determined from the Crystallographic Work of Sundaralingam and Putkey[10] and from the Experimental Eigenvectors for the hfc Tensors of Radical I

		H4−C2−C3 = 120°	
angle	crystallographic	experimental	difference
H2−C2−H3	51.9°	48.5°	3.4°
H2−C2−C3	27.7°	23.9° #2	3.8°
H3−C2−C3	30.9°	25.4° #3	5.5°

The new C2−C3 bond direction found from the hfc tensors of radical **I** makes it possible to calculate the expected dihedral angles of the β-protons H2 and H3. This calculation yields $\theta_2 = 6.70°$ and $\theta_3 = 141.6°$. The agreement with the values estimated on the basis of the hfc isotropic values above is satisfactory.

4.2. Radical II. From the FSE experiments, three of the ENDOR determined hfc tensors have been ascribed to radical **II**. Tensor #4 represents a coupling to a nonexchangeable proton and is clearly of α-type. Combined with the observation that the *g*-tensor is virtually isotropic, this requires that the LEO is located at one of the carbon atoms C2 or C3.

The exchangeable proton responsible for the hfc coupling #6 must be one of the amino protons, but the coupling tensor does not, at first look, give an answer if this is a β- or γ-type hfc. Also, the nitrogen hfc tensor #5 does not directly indicate the localization of the LEO. However, knowledge of the relative signs of the ^{14}N hyperfine and quadrupolar tensors, combined with an estimate of the absolute sign of the quadrupolar tensor, yields the sign of the ^{14}N hfc tensor, which in turn tells if it is an α- or β-type tensor. This will be done below (section 4.3).

Regardless of the localization of the LEO, the spin density at the central atom can be calculated from tensor #4. Using the McConnell relation[14] with $Q^H_{CH} = -73.4$ MHz,[15] the isotropic value $a_{iso} = -51.0$ MHz gives $\rho^\pi_{iso} = 0.695$. The McConnell relation is valid only if the C atom has rehybridized to a planar sp^2 configuration.[16] The Gordy−Bernhard method[17] gives $\rho^\pi_{dip} = 0.793$ from the dipolar tensor, which is 14% larger than ρ^π_{iso}. This indicates that the configuration of the central atom deviates from pure sp^2 hybridization and that ρ^π_{dip} is the better estimate for the LEO spin density.

Firstly, assume that the LEO is located at C2. In addition to the hfc tensors #4, #5, and #6, the FSE spectra show that at least one more coupling, almost undetectable in ENDOR, must be present. If it is just one significant coupling, this interaction must have tensor elements close to those of tensor #7 in Table 2, which is a β-type coupling to a nonexchangeable proton. Tensor #7 has $a_{iso} = 25$ MHz, a value, however, with considerable uncertainty. With a spin density of $\rho^\pi = 0.793$, the Heller−McConnell relation[18] gives a dihedral angle of $\theta = 68.1°$ with $B_0 = +14.0$ MHz and $B_2 = 126$ MHz.[19] (For the present discussion, nonplanarity of the radical center is not taken into account for the discussion of proton β-coupling interactions.) If the LEO is localized on C2, the #7 coupling must be a coupling with either H3 or H2. The difference between the dihedral angles of these two protons is 120°. From the direction of the LEO, assumed to be parallel to the eigenvector for the intermediate principal value of tensor #4, it is found that the dihedral angles of H2 and H3 (using the crystallographic bond directions) are 1.9° and 129.0° (51.0°). A β-coupling with dihedral angle close to 0° would give a large coupling which easily should be observed in the FSE spectra. The failure to do so argues against the LEO being localized on C2.

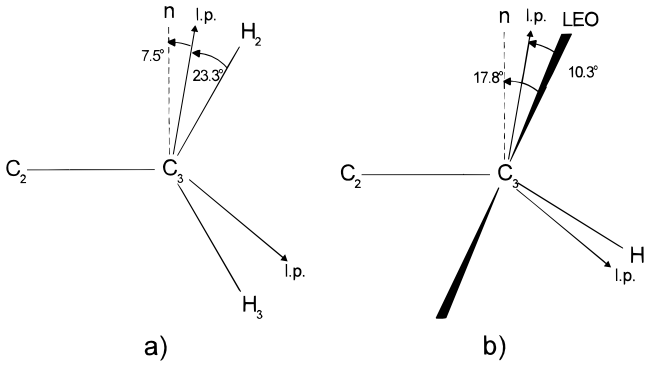

Figure 10. C2−C3−O1 fragment in L-*O*-serine phosphate single crystals as seen along the C3−O1 bond. (a) The projection of the lone pairs (1p, straight arrows) at O1 into the plane of the paper, together with the vector *n*, the normal to the plane spanned by C2−C3−O1, and the C3−H2 and C3−H3 bonds before radical formation. (b) The same situation in radical **II** with H2 removed and replaced by LEO rotated into its stable orientation.

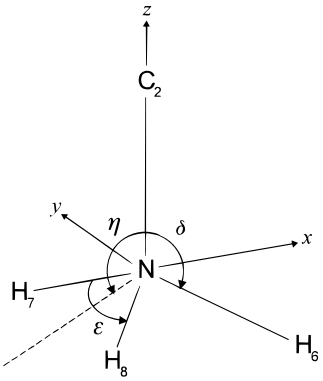

Figure 11. Geometry around the nitrogen atom in L-*O*-serine phosphate with the reference coordinate system (*x*,*y*,*z*) and the definition of the angles ϵ, δ, and η used for the discussion of quadrupolar couplings in radical **II**.

If the LEO is localized at C3, the LEO direction from tensor #4 and the crystallographic data show that the dihedral angle of H4 is 59.7°, which is in reasonable agreement with the calculated value, 68.1°, for tensor #7. The FSE spectra also show that the maximum value of this coupling occurs close to the *a*-axis. The H4−C3 direction is only 21° from this axis.

The eigenvector of the intermediate principal value of tensor #4 defines the direction of the LEO.[8] The angle between this direction and the direction perpendicular to the plane defined by C2−C3−O1 is 19.5°. If the configuration of C3 was pure sp^2, these two directions should have been parallel. If the LEO is localized at C3, the radical must have been formed upon abstraction of either H2 or H3. It is assumed that when the C−H bond is broken, the initially sp^3-hybridized C3 atom will try to attain an sp^2 configuration by rotation of the LEO in the plane defined by H2−C3−H3. This is consistent with the fact that the LEO and the eigenvector of the smallest principal value of tensor #4 are both almost in this plane (the angles with the perpendicular to the plane are 83.3° and 87.8°, respectively). Upon further discussion it is assumed and confirmed that the LEO is localized at C3 and that radical **II** exhibits the structure

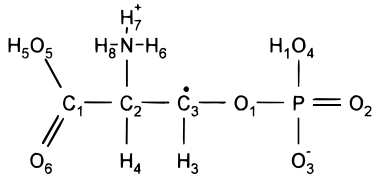

Radical II

It seems clear that C3 does not exhibit a pure sp^2 configuration. Thus, the radical center is slightly pyramidal and the LEO exhibits a small 2s orbital character. Incomplete rehybridization is not unusual in carbon-centered radicals with oxygen atoms as nearest neighbors. Dobbs *et al.*[16,20] have observed this in oxy-substituted alkyl radicals and have reported smaller than expected numerical values for isotropic values for α-couplings. This was explained by a 2s orbital contribution to the LEO because of the deviation from planar hybridization. The same radical structure as that suggested for radical **II** observed in this work was observed by Sørnes *et al.*[8] in AES.

Worth and Richards[21] have explained this effect by *ab initio* molecular-orbital calculations with the presence of the lone-pair (lp) orbitals at the neighboring oxygen atom which interact with the LEO by electrostatic repulsion. In Figure 10a the situation in SP as seen along the C3−O1 bond is illustrated. One of the lp's of O1 is oriented between the perpendicular to the C2−C3−O1 plane and the broken C−H bond and thereby prohibits the LEO from attaining the sp^2 configuration. The result is a pyramidal structure as visualized in Figure 10b, which is the situation in radical **II**. This argument is valid only if it is the H2−C3 bond that breaks upon radical formation. This appears to be so from the following argument.

Radical **II** is the result of removing one of the H atoms bonded to C3. It is assumed that the LEO is closest to the direction of the C−H bond from which it originates. The H2−C3 bond direction and the LEO form an angle of 20.0°, while the corresponding angle between the LEO and the C3−H3 bond direction is 44.4°. It therefore seems reasonable that radical **II** is formed by the net loss of H2 from SP.

4.3. The ^{14}N Hyperfine and Quadrupolar Coupling. The Townes−Dailey approximation[22] yields a method to estimate the quadrupolar tensor. For the nitrogen atom, only the $2p_x$, $2p_y$, and $2p_z$ orbitals are to be considered in the Townes−Dailey approximation. With a basis as shown in Figure 11, Böttcher *et al.*[23] (Sørnes *et al.*[8] have called attention to some errors in ref 23, which are corrected in eq 2) defined the bonding orbitals of the nitrogen atom and thereby the tensor elements to be

$$Q_{xx} = -\frac{e^2Q}{4\pi\epsilon_0 2I(2I-1)h}a_0[-1/2\sin^2\alpha\sigma_C - 1/2\sin^2\beta(3\sin^2\delta - 1)\sigma_{H6} + 1/2\sin^2\gamma(3\cos^2(\epsilon/2)\sin^2\eta - 1)(\sigma_{H7} + \sigma_{H8})]$$

$$Q_{yy} = -\frac{e^2Q}{4\pi\epsilon_0 2I(2I-1)h}a_0[-1/2\sin^2\alpha\sigma_C - 1/2\sin^2\beta\sigma_{H6} + 1/2\sin^2\gamma(3\sin^2(\epsilon/2) - 1)(\sigma_{H7} + \sigma_{H8})]$$

$$Q_{zz} = -\frac{e^2Q}{4\pi\epsilon_0 2I(2I-1)h}a_0[\sin^2\alpha\sigma_C - 1/2\sin^2\beta(\cos^2\delta + 1)\sigma_{H6} - 1/2\sin^2\gamma(\cos^2(\epsilon/2)\cos^2\eta + 1)(\sigma_{H7} + \sigma_{H8})] \quad (2)$$

$$Q_{xy} = -\frac{e^2Q}{4\pi\epsilon_0 2I(2I-1)h}a_0[-3/4\sin^2\gamma\sin\eta\sin\epsilon(\sigma_{H7} - \sigma_{H8})]$$

$$Q_{yz} = -\frac{e^2Q}{4\pi\epsilon_0 2I(2I-1)h}a_0[-3/4\sin^2\gamma\cos\eta \sin\epsilon(\sigma_{H7}-\sigma_{H8})]$$

$$Q_{zx} = -\frac{e^2Q}{4\pi\epsilon_0 2I(2I-1)h}a_0[3/4\sin^2\beta\sin 2\delta\sigma_{H6} - 3/4\sin^2\gamma\sin 2\eta\cos^2(\epsilon/2)(\sigma_{H7}+\sigma_{H8})]$$

where σ_k denotes the valence orbital coefficient (electron population) in the bonding molecular orbital modeling the kth bond (assuming a RHF model), the angles ϵ, δ, and η are defined in Figure 11, and the angles α, β, and γ are obtained by orthogonality requirements to be

$$\tan^2\alpha = -\frac{\cos(\delta+\eta)}{\cos\eta\cos\delta}$$

$$\tan^2\beta = -\frac{\cos\eta}{\cos(\delta+\eta)\cos\delta} \qquad (3)$$

$$\tan^2\gamma = -\frac{\cos\delta}{\cos(\delta+\eta)\cos\eta\cos^2(\epsilon/2)}$$

The factor $-[e^2Q/4\pi\epsilon_0 2I(2I-1)h)]a_0$ has a value between -5.0 and -4.0 MHz.[24] In this work -4.5 MHz has been used.

In a perfectly tetrahedral amino group ϵ and δ are 109.47° and η is 125.26°. Equation 2 then gives an axially symmetric quadrupolar tensor which only depends on differences in the electron populations of the bonding orbitals at the nitrogen atom. However, deviation from tetrahedral structure will also make actual populations significant variables and axial symmetry may disappear.

Sørnes *et al.*[8] have observed an axially symmetric quadrupolar coupling for the nitrogen atom of the amino group in AES. The asymmetry parameter η was only 0.095. (The asymmetry parameter is defined by McDowell and Naito[25] as $(Q_{aa}-Q_{bb})/Q_{cc}$ with $|Q_{aa}| \le |Q_{bb}| \le |Q_{cc}|$.) In the present work, Table 2 shows that $\eta = 0.379$, far too large to categorize the quadrupolar tensor as axially symmetric. In glycine Deigen *et al.*[26] have found a quadrupolar tensor for the amino group with an even larger asymmetry. Several reasons for this behavior may be suggested and tested. One possibility is that the amino group has rehybridized to sp^2 upon deprotonation. A deprotonation can also occur without any rehybridization since the hydrogen bonding in the amino group could conserve the sp^3 configuration. In both cases a lone-pair orbital is formed which will be the dominating direction and remove the axial symmetry of the quadrupolar tensor. Both models have been tested without obtaining convincing agreement with the experimental data. Another possible reason for the nonaxial symmetry of the quadrupolar tensor is a deviation from tetrahedral configuration of the amino group by differences in the electronic populations of three H−N bonds. If the quadrupolar tensor is rotated to a basis as shown in Figure 11, the following result is obtained:

$$\mathbf{P} = \begin{bmatrix} -0.469 & -0.174 & 0.004 \\ -0.174 & -0.390 & -0.240 \\ 0.004 & -0.240 & 0.858 \end{bmatrix} \qquad (4)$$

This tensor has an asymmetry parameter of only $\eta = 0.092$. With values of ϵ, δ, and η corresponding to a perfect tetrahedral structure, eq 2 shows that the nondiagonal elements of the quadrupolar tensor only depend on differences in the electron population of the H−N bonds. With a value of $\sigma_{H6} = b$ in eq 2, the expression for the nondiagonal elements of **P** in eq 4 yields $\sigma_{H7} = b - 0.067$ and $\sigma_{H8} = b + 0.062$. (The Q_{xy} and Q_{yz} elements of eq 4 give different answers for the difference between σ_{H7} and σ_{H8}: -0.089 and -0.1743. The mean value is used in this work.) These differences are both small and indeed possible, considering the variations in bond lengths and hydrogen bonding. The diagonal elements of eq 4 give an estimate for the differences in electron population in the C−N bonding orbital. With $\sigma_C = a$, the results are $a - b = -0.276$ for Q_{xx}, $a - b = -0.236$ for Q_{yy}, $a - b = -0.256$ for Q_{zz}, and the mean is $a - b = -0.256$.

The result that b is greater than a is explained by taking into account that the electron distribution in a bond depends on the electronegativity of the different atoms constituting this bond.[8] The electronegativity is for N 3.0, for C 2.5, and for H 2.1.[27] This results in the carbon atom taking more of the electrons in the C−N bond than the protons in the H−N bonds, and thus the electron populations in the bonding orbitals of N to H become greater than that in the orbital of N to C. This confirms the sign of the quadrupolar tensor used in Table 2. Furthermore, this confirms the positive isotropic value of the nitrogen hfc and consequently the localization of the LEO to C3.

The dihedral angle of the N atom with respect to the direction of the LEO is found to be $\theta_N = 42.1°$, using the crystallographic data combined with the experimental direction of the LEO. In the same way as for the Heller−McConnell relation for β-protons (eq 1 above) this value should be associated with the nitrogen isotropic value of $a_{iso} = 15.89$ MHz. While the constants B_0 and B_2 are well-known for β-protons, they are far less known for β-nitrogen couplings, although some theoretical estimates using INDO calculations have been done by Close *et al.*[28] The corresponding values observed in an equivalent radical in AES[8] is $\theta_N' = 10.5°$, $a_{iso'} = 26.3$ MHz, and $\rho'_{dip} = 0.765$. If a model as simple as $a_{iso} = B_2\cos^2\theta\rho^\pi$ is used, the two systems give the constants $B_2 = 36.4$ MHz and $B_2' = 35.6$ MHz. If a constant $B_0\rho^\pi$ is added to the model, as in the Heller−McConnell relation (eq 1), the two systems together give $B_0 = 1.0$ MHz and $B_2 = 34.5$ MHz. Due to the nonplanar nature of the radical center, a first-order term is expected[29] to contribute in the expression, which then will take the form

$$a_{iso} = \rho^\pi(B_0 + B_1\cos\theta + B_2\cos^2\theta) \qquad (5)$$

The present data combined with those for AES[8] yield only two parameters of this equation. Since B_0 is expected to be small, it is arbitrarily set to zero. The calculations then yield estimated values of the constants $B_1 = 2.6$ MHz and $B_2 = 32.9$ MHz.

The dipolar tensor of the ^{14}N coupling (2.06, -0.27, -1.82) MHz deviates from axial symmetry with an asymmetry parameter of $\eta = 0.752$. In addition, the directions of the C3−N bond and the eigenvector for the largest principal value of the ^{14}N hfc tensor deviate by 21.8°. The explanation must be that the dipolar coupling to an N atom as a part of an amino group cannot necessarily be compared with the dipolar coupling to an H atom. This is illustrated by the following attempt to reconstruct the dipolar coupling tensor.

The spin at C3 contributes to an axially symmetric β-type tensor with principal elements (0.62, -0.31, -0.31) MHz. This is calculated from the LEO spin density of 0.793, using the point-dipole model for proton β-couplings suggested by Zeldes *et al.*[30] and scaled with a factor 0.07[31] according to the ratio of the nuclear g-factors of N and H.

The spin localized in the 2p orbitals of the nitrogen will also contribute to the dipolar tensor. The spin density in these 2p orbitals is calculated as follows. From the isotropic value 15.89 MHz the nitrogen 2s population is obtained by scaling with the constant 1811 MHz[32] and becomes 0.008 77. The s/p ratios

for the valence orbitals are obtained from the model of Böttcher *et al*. (eq 2) and give 2p spin densities of 0.0332 for the C2−N bond and 0.0250, 0.0265, and 0.0265 for the H6−N, H7−N, and H8−N bonds, respectively. With unit spin density in a 2p orbital the dipolar tensor is (95.6, −47.8, −47.8) MHz[33] with the symmetry axis along the 2p orbital direction. In the laboratory frame of reference, the complete dipolar tensor composed of all nitrogen 2p orbital contributions above then becomes

$$\begin{bmatrix} 0.164 & 0.730 & 0.267 \\ 0.730 & -0.004 & 0.055 \\ 0.267 & 0.055 & -0.165 \end{bmatrix} \quad (6)$$

Taken together with the contribution from the carbon atom this gives a diagonalized dipolar tensor with principal values of (1.36, −0.41, −0.95) MHz. This tensor has principal values about half of those for the experimental ones. Furthermore, the eigenvector of the largest value deviates from the observed direction by 30°.

However, by varying the spin densities in the N−H bonds, it is found that with 0.0175, 0.0186, and 0.0106 as 2p contributions in the H6−N, H7−N, and H8−N bonds a dipolar tensor of (2.61, −0.66, −1.95) MHz is obtained, with eigenvectors which deviated from the observed ones by only 1.6°, 1.8°, and 3.1°, respectively. This shows that small variations in the 2p spin densities induced by the environment can give a dipolar tensor which reproduces that observed.

4.4. Radical III. From the FSE experiments, two of the ENDOR determined hfc tensors were associated with radical **III**. Both couplings are due to nonexchangeable protons of the α-type. In addition the FSE spectra reveal that at least one more coupling contributes to the resonance. The two α-couplings are similar and of a magnitude such that the responsible protons both must be bonded to the same carbon atom. It is consequently assumed that the LEO is localized at C3.

Radical **III** is suggested to be the result of scission of either the C3−O1 bond or the C2−C3 bond. This will, in both cases, lead to rehybridization at C3 from an sp^3 to an sp^2 configuration. The LEO will be perpendicular to the plane defined by the sp^2 hybrid orbitals. The eigenvectors for the intermediate principal values of the two α-tensors, which represent the direction of the LEO, deviate only 3.3° from each other. This confirms that the two protons are bonded to the same atom. In the following discussion, the eigenvector for the intermediate principal value of tensor #8 is taken to denote the direction of the LEO.

As mentioned above, radical **III** may be formed by the scission of either the C2−C3 bond or the C3−O1 bond. In the case of breakage of the C2−C3 bond, the angle between LEO and C3−O1 should be close to 90° if the geometry of the C3−O−PO_3^-H fragment is preserved. However, this angle (which depends upon the signs of the eigenvectors used) can not be smaller than 124°. On the other hand, breakage of the C3−O1 bond gives the corresponding angle between the LEO and the C2−C3 bond as small as 96.3°. The eigenvectors for the smallest principal values of the α-tensors are expected to be along the directions of the C−H bonds. From this, the angle between the C−H direction of tensor #8 and the crystallographic C3−C2 bond direction is 124.6°, the corresponding angle for tensor #9 is 119.6°, and finally, the angle between the two C−H directions given by #8 and #9 is 115.7°. The sum of these three angles is 359.9°, which confirms the sp^2 configuration at C3.

These considerations all lead to the conclusion that radical **III** is a result of the cleavage of the C3−O1 bond. The angle between the eigenvector of the smallest principal value of tensor #9 and the crystallographic C3−H3 direction is 17.3°, and for tensor #8 the corresponding angle with C3−H2 is 56.1°. If minimum reorientation of the molecule upon radical formation is assumed, tensor #8 must represent the interaction with H2, while tensor #9 represents the interaction with H3.

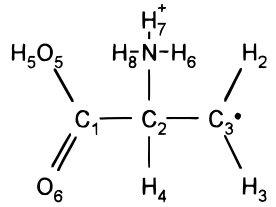

Radical III

From the radical structure, couplings to the amino group and to H4 are expected. The McConnell relation and the isotropic value of hfc tensor #8 give a spin density at C3 of $\rho^{\pi}_{iso} = 0.690$. The Gordy−Bernhard method[17] gives $\rho^{\pi}_{dip} = 0.672$ from the dipolar tensor, which is close to ρ^{π}_{iso} and confirms the sp^2 configuration. Using the experimental direction for the LEO and crystallographic data for the coordinates of H4, the dihedral angle of H4 is $\theta = 33.5°$. By the Heller−McConnell relation (eq 1) with $\rho^{\pi} = 0.690$, $B_0 = 0$, $B_2 = 126$ MHz, and $\theta = 33.5°$ an expected isotropic value of 73.0 MHz is calculated for the coupling to H4. The expected principal dipolar tensor elements are (13.3, −6.6, −6.6) MHz using the point-dipole approximation.[30] If the extra coupling, missing in the ENDOR spectra but clearly present in the FSE spectra, is a coupling to a proton, it should be 71.4 MHz for the *b*-axis orientation, which fits nicely with the above calculations for the expected β-coupling to H4. On the other hand, the dihedral angle of N is 84.9°, and any significant coupling to this atom is not expected. This leads to the conclusion that the missing coupling in the FSE spectra from radical **III** is a β-coupling to H4. It is interesting that also in radical **II** the β-coupling to H4 was difficult to observe by ENDOR. This probably reflects particularly favorable relaxation properties due to a particular environment of this nucleus, which may be probed by studies at lower temperature.

5. Mechanistic Aspects

All three radicals are localized at the serine part of SP, and the equivalent species have been observed in irradiated single crystals of serine.[9,10] This indicates that the phosphate group in SP does not significantly affect the radiation chemistry of serine. This must be ascribed to the presence of the carboxyl group which apparently acts as an effective electron, as well as hole, scavenger. The formation mechanisms of the corresponding radicals in serine have been thoroughly investigated,[9,10] and there are no experimental indications that the mechanisms are not essentially the same in SP. Thus, the radicals observed in the present work are suggested to be formed as outlined below.

5.1. Radical I. A radical with structure equivalent to that of radical **I** in SP was found in serine by Lebedev and Almanov at 300 K.[9] This was later conformed by Castleman and Moulton.[10] These authors used temperature variation experiments to show that this radical is a secondary product of the primary reduction species. On the basis of this, the formation mechanism of radical **I** is suggested to be as shown in Figure 12.

5.2. Radical II. A radical of structure equivalent to radical **II** in SP was observed in serine by Castleman and Moulton.[10] In serine this species is believed to be formed both as a secondary product of the equivalent of radical **I**, which decays

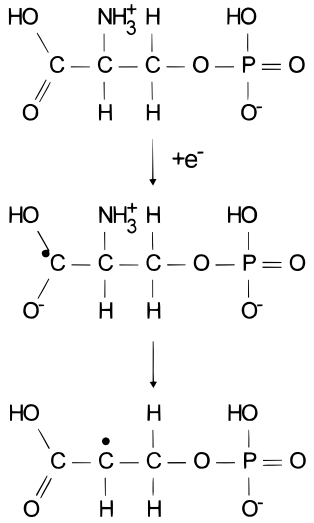

Figure 12. Proposed mechanism of formation of radical **I**.

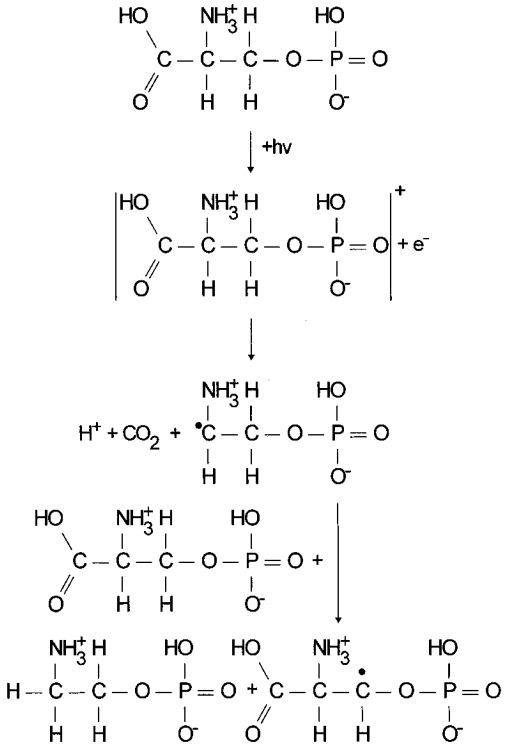

Figure 13. Proposed mechanism of formation of radical **II**.

upon heating, and as a secondary radical from the primary oxidation product. In the latter case, the secondary radical is formed already at 153 K. Both mechanisms proceed by intermolecular hydrogen abstraction. Thermal decay of radical **I** resulting in radical **II** is not observed in the present work. This makes it most probable that radical **II** is a secondary radical from the primary oxidation product, and a formation mechanism is suggested as shown in Figure 13.

5.3. Radical III. Radical **III** has no equivalent radical in serine as judged from the 300 K studies.[10] However, Lee and Box[9] observed a third primary product with the same structure as radical **III** by X-irradiation and observation at 4.2 K. In SP there is little experimental evidence for the precursor of this radical. One possibility is that the formation of radical **III** in SP may follow from a primary phosphoranyl radical, as observed formed in other dialkyl or dihydroxyalkyl phosphates[3,6,7,34] following reduction of the phosphate group. The phosphoranyl radical was, however, not observed in polycrystalline SP after

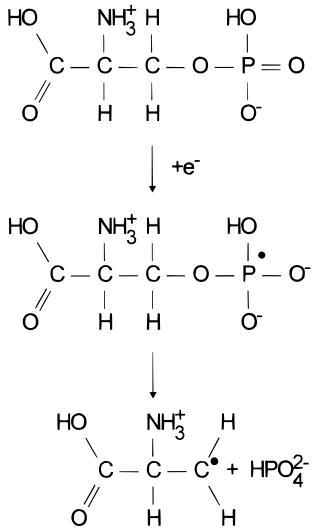

Figure 14. Proposed mechanism of formation of radical **III**.

irradiation and observation at 77 K. Thus, this eventually formed phosphoranyl radical must be unstable and must decay prior to observation at 77 K by phosphate elimination. According to this model, a formation mechanism as that shown in Figure 14 is suggested. This model should be tested by low-temperature experiments.

Acknowledgment. The writing of this paper was facilitated by a travel scholarship to A.S. granted by the Nordic Academy for Research Education, NorFA. Prof. A. Lund is thanked for his hospitality during the 2 month visit in Linköping, Sweden. Prof. D. M. Close is acknowledged for suggesting this problem. Mr. A. R. Sørnes is acknowledged for making the analysis of the quadrupolar couplings possible and for helpful discussions.

References and Notes

(1) Becker, D.; Sevilla, M. D. *Adv. Radiat. Biol*. **1993**, *17*, 121.
(2) Bernhard, W. A.; Barnes, J.; Mercer, K. R.; Mroczka, N. *Radiat. Res*. **1994**, *140*, 199.
(3) Nelson, D. J.; Symons, M. C. R.; Wyatt, J. L. *J. Chem. Soc., Faraday Trans*. **1993**, *89*, 1955.
(4) Boon, P. J.; Cullis, P. M.; Symons, M. C. R.; Wren, B. W. *J. Chem. Soc., Perkin Trans. 2* **1984**, 1393.
(5) Bungum, B.; Hole, E. O.; Sagstuen, E.; Lindgren, M. *Radiat. Res*. **1994**, *139*, 194.
(6) Sanderud, A.; Sagstuen, E. *J. Chem. Soc., Faraday Trans*. **1996**, *92*, 995.
(7) Fouse, G. W.; Bernhard, W. A. *J. Chem. Phys*. **1979**, *70*, 1667. Fouse, G. W. Thesis submitted for the degree Ph.D. at the Department of Radiation Biology and Biophysics, University of Rochester, Rochester, New York, 1979.
(8) Sørnes, A. R.; Sagstuen, E. *J. Phys. Chem*. **1995**, *99*, 16857. Sørnes, A. R.; Sagstuen, E.; Lund, A. *J. Phys. Chem*. **1995**, *99*, 16867.
(9) Lee, J. Y.; Box, H. C. *J. Chem. Phys*. **1973**, *59*, 2509. Lebedev, Ya.; Almanov, G. A. *Biofizika* **1967**, *12*, 338.
(10) Castleman, B. W.; Moulton, G. C. *J. Chem. Phys*. **1971**, *55*, 2598. Castleman, B. W.; Moulton, G. C. *J. Chem. Phys*. **1972**, *57*, 2762.
(11) Sundaralingam, M.; Putkey, E. F. *Acta Crystallogr*. **1970**, *B26*, 790.
(12) Nelson, W. H. *J. Magn. Reson*. **1980**, *38*, 71.
(13) Schonland, D. S. *Proc. Phys. Soc. (London)* **1958**, *73*, 788.
(14) McConnell, H. M. *J. Chem. Phys*. **1965**, *24*, 764.
(15) Fessenden, R. W.; Schuler, R. H. *J. Chem. Phys*. **1963**, *39*, 2147.
(16) Dobbs, A. J.; Gilbert, B. C.; Norman, O. C. *J. Chem. Soc. A* **1971**, 124.
(17) Gordy, W. *Theory and applications of spin resonance*; John Wiley & Sons: New York, 1980. Bernhard, W. A. *J. Chem. Phys*. **1965**, *24*, 764.
(18) Heller, C.; McConnell, H. M. *J. Chem. Phys*. **1960**, *32*, 1535.
(19) Morton, J. R. *J. Chem. Rev*. **1964**, *64*, 453.
(20) Dobbs, A. J.; Norman, O. C.; Gilbert, B. C. *J. Chem. Soc., Perkin Trans. 2* **1972**, 786.
(21) Worth, G. A.; Richards, W. G. *J. Am. Chem. Soc*. **1987**, *116*, 239.

(22) Townes, C. H.; Dailey, B. P. *J. Chem. Phys.* **1949**, *17*, 782.
(23) Böttcher, R.; Metz, H.; Windsch, W. *J. Chem. Phys.* **1985**, *93*, 137.
(24) Schweiger, A. *Struct. Bonding* **1982**, 51.
(25) McDowell, C. A.; Naito, A. *J. Magn. Reson.* **1981**, *45*, 205.
(26) Deigen, M. F.; Krivenko, V. G.; Pulatova, M. K.; Ruban, M. A.; Teslenko, V. V.; Kayushin, L. P. *Biophysics* **1973**, 242.
(27) Atkins, P. W. *General Chemistry (International Student Edition)*; Scientific American Books: W. H. Freeman & Co.: New York, 1989.
(28) Close, D. M.; Fouse, G. W.; Bernhard, W. A.; Andersen, R. S. *J. Chem. Phys.* **1979**, *70*, 2131.
(29) Colson, A. O.; Sevilla, M. D. *Int. J. Radiat. Biol.* **1995**, *67*, 627.
(30) Zeldes, H.; Trammell, G.; Livingston, R.; Holmberg, R. *J. Chem. Phys.* **1960** *32*, 618.
(31) Weil, J. A.; Preston, K. F. *BRUKER EPR/ENDOR Frequency Table*, BRUKER EPR spectrometer accompaniment.
(32) Morton, J. R.; Preston, K. F. *J. Magn. Reson.* **1978**, *30*, 577.
(33) Morton, J. R.; Rowlands, J. R.; Whiffen, D. H. Atomic Properties for Interpreting ESR Data, National Physics Laboratory, BPR 13, 1962.
(34) Nelson, D. J.; Symons, M. C. R. *J. Chem. Soc., Perkin Trans. 2* **1977**, 286.

JP960063X